ISSN 0915-633X

NATIONAL INSTITUTE FOR FUSION SCIENCE

Effects of Net Toroidal Current on Mercier Criterion in the Large Helical Device

K. Ichiguchi, N. Nakajima, M. Okamoto, Y. Nakamura
and M. Wakatani

(Received – Aug. 17, 1992)

NIFS-174 Sep. 1992

RESEARCH REPORT
NIFS Series

NAGOYA, JAPAN

Effects of Net Toroidal Current on Mercier Criterion in the Large Helical Device

Katsuji Ichiguchi, Noriyoshi Nakajima, Masao Okamoto
National Institute for Fusion Science,
Nagoya 464-01, Japan

Yuji Nakamura, Masahiro Wakatani
Plasma Physics Laboratory,
Kyoto University,
Gokasho, Uji 611, Japan

Abstract

Effects of the net toroidal current on the local ideal MHD stability or the Mercier criterion are investigated for a plasma in the heliotron/torsatron configuration by taking the Large Helical Device as an example. The three dimensional equilibrium code, VMEC, is used to study the local stability of equilibria with given net toroidal current. It is found that a subtractive current which decreases the rotational transform improves the stability while an additive current which increases the rotational transform deteriorates the stability. The change of the rotational transform at the magnetic axis due to the net toroidal current is the essential mechanism for the change of the stability property. Stability diagrams are drawn against the Mercier criterion for the configuration of the Large Helical Device shifting the plasma position inward or outward.

Keywords

MHD stability, Mercier criterion, Large Helical Device, net toroidal current, Shafranov shift, plasma position

1 Introduction

Since heliotron/torsatron configurations have an advantage that there exist equilibria without a net toroidal current, most of MHD stability analyses have been concentrated to the currentless equilibria[1]. As for the cases with net toroidal currents, only the flux-conserving equilibria have been studied systematically in these configurations. In practice, however, some other net toroidal currents such as the bootstrap current, the beam-driven current (Ohkawa current), or the RF-induced current may flow even in the plasma after the relaxation from the flux conserving stage for a long pulse operation.

Among various toroidal currents the bootstrap current is especially important since it is generated without any external current driving source. It is well known that the bootstrap current has a strong dependence on the magnetic field configuration in the non-axisymmetric toroidal system[2, 3]. Three-dimensional MHD equilibria including the bootstrap current self-consistently have been studied for the Large Helical Device[4]. It was shown in this paper that the bootstrap current flows in the direction increasing the rotational transform and reducing the Shafranov shift. Total bootstrap current estimated for the plasma with $\langle\beta\rangle \simeq 1\%$ ($\langle\beta\rangle$ is the averaged beta value) in the LHD configuration easily exceeded 100 kA under the assumption that both ions and electrons belong to the limit of the $1/\nu$ collisionality regime in the whole plasma region[4].

Recently the neoclassical theory for the parallel flow, current, and rotation has been extended to a multi-species plasma in general toroidal systems[5] to explore the difference between rotations of bulk ions and impurity ions[6] and the effect of external momentum sources of fast ions and an inductive electric field[7]. The extended theory has revealed that the parallel current generated directly by the radial electric field, which does not exist in the axisymmetric system, exists in the non-axisymmetric system if electrons and ions have different collisionalities[5, 8]. This newly found current generation mechanism has a possibility to reverse the direction of the bootstrap current flow if the radial electric field is sufficiently large.

In the beam-induced current case, The direction of the beam-induced current is determined by the injection angle and the current density profile depends on the deposition

profile. The RF-induced current also depends on the deposition profile and the direction can be changed according to the momentum input.

On the other hand, Morimoto et al. carried out experiments with induced current by the Ohmic coils in the Heliotron DR device[9]. They observed MHD fluctuations in the soft X-ray and Mirnov coil signals, and showed that the fluctuations were considerably reduced by the Ohmic current decreasing the edge rotational transform by about 10% while the current in the opposite direction enhanced the fluctuations.

Thus the net toroidal current may affect the MHD stability in heliotron/torsatron configurations. It is crucial to investigate theoretically how the net toroidal current changes the MHD stability properties. In this paper we study the effects of net toroidal currents on the local ideal MHD stability or the Mercier criterion for the plasma in the heliotron/torsatron configuration of the Large Helical Device[10], which is constructed in the National Institute for Fusion Science. We focus the equilibria after the relaxation from the flux-conserving stage because the LHD is designed for the steady-state or long-pulse operation. We apply the three dimensional equilibrium code, VMEC code[11], to this problem. In order to understand the basic mechanism changing the MHD stability properties, three cases are considered for a fixed profile of the current density; the case of a subtractive net toroidal current flowing in the opposite direction of the helical coil current or decreasing the rotational transform, the currentless case, and the case of an additive net toroidal current flowing in the direction of the helical coil current or increasing the rotational transform. Stability diagrams are drawn against the Mercier criterion by changing the plasma position outward or inward.

2 Calculation of Mercier Criterion

We investigate the local ideal MHD stability or the Mercier criterion for the plasma in the Large Helical Device (LHD)[10] using the three-dimensional equilibrium code VMEC. The Mercier criterion[12, 13, 14] for stability is given by

$$D_M = D_S + D_{MW} + D_G > 0, \tag{2.1}$$

where

$$D_S = \frac{\iota'^2}{4}, \tag{2.2}$$

$$D_{MW} = \left\langle \left[P'V'' - P'^2 \left\langle \frac{1}{\mathbf{B}^2} \right\rangle + \iota'(I' - \sigma) \right] \frac{\mathbf{B}^2}{|\nabla\Phi|^2} \right\rangle, \tag{2.3}$$

$$D_G = \left\langle \frac{\sigma \mathbf{B}^2}{|\nabla\Phi|^2} \right\rangle^2 - \left\langle \frac{\mathbf{B}^2}{|\nabla\Phi|^2} \right\rangle \left\langle \frac{\sigma^2 \mathbf{B}^2}{|\nabla\Phi|^2} \right\rangle. \tag{2.4}$$

In these equations, $\mathbf{B}$, $\mathbf{J}$, P and ι are the magnetic field, the current density, the plasma pressure, and the rotational transform, respectively. V is the volume of a magnetic flux tube. Φ and I are the toroidal flux and the total toroidal current within a magnetic flux tube given by

$$\Phi = \frac{1}{2\pi} \int \mathbf{B} \cdot \nabla\zeta dV, \tag{2.5}$$

$$I = \frac{1}{2\pi} \int \mathbf{J} \cdot \nabla\zeta dV, \tag{2.6}$$

where ζ denotes a toroidal angle. In Eqs.(2.3) and (2.4), $\langle f \rangle$ denotes the flux average of a quantity f defined by

$$\langle f \rangle \equiv \frac{d}{d\Phi} \int f dV. \tag{2.7}$$

Here we use the unusual definition of Eq.(2.7) for the flux average because of the simplicity of the expressions in Eqs.(2.3) and (2.4). The prime denotes the derivative with respect to Φ ($' \equiv d/d\Phi$), and σ is defined by

$$\sigma = \frac{\mathbf{J} \cdot \mathbf{B}}{\mathbf{B}^2}. \tag{2.8}$$

This quantity includes Pfirsch-Schlüter current and net toroidal current, and satisfies the magnetic differential equation,

$$\frac{\mathbf{B} \cdot \nabla\sigma}{P'} = \frac{2\mathbf{B} \times \nabla\Phi \cdot \boldsymbol{\kappa}}{\mathbf{B}^2}. \tag{2.9}$$

Here κ denotes the curvature of the line of force defined by

$$\kappa = \frac{\mathbf{B}}{|\mathbf{B}|} \cdot \nabla \frac{\mathbf{B}}{|\mathbf{B}|}. \tag{2.10}$$

Eq.(2.9) means that σ is related to the geodesic curvature of the line of force.

Here we use the expression of the Mercier criterion divided into three terms as seen in Eqs.(2.2) to (2.4). The first term given by D_S is the magnetic shear term which always has a stabilizing contribution. We call the second term, D_{MW}, the modified well term. According to Ref.[13], this term can be considered to be composed by the two terms given by

$$D_{MW} = D_W + D_{J\cdot B}, \tag{2.11}$$

$$D_W = P' \left(V'' - P' \left\langle \frac{1}{\mathbf{B}^2} \right\rangle \right) \left\langle \frac{\mathbf{B}^2}{|\nabla \Phi|^2} \right\rangle, \tag{2.12}$$

$$D_{J\cdot B} = \iota' \left\langle \frac{(I' - \sigma)\mathbf{B}^2}{|\nabla \Phi|^2} \right\rangle. \tag{2.13}$$

The first term in D_W represents the magnetic well effect. In the case of a usual pressure profile with $P' < 0$, $V'' < 0$ is favorable for the stability which corresponds to the magnetic well. The second term in D_W term means the correction by the diamagnetic effect. The $D_{J\cdot B}$ term consists of the net toroidal current and σ parts. This term can be positive or negative depending on the sign of the magnetic shear of ι'. As is seen in the expression of Eq.(2.3), the $D_{J\cdot B}$ term can be recognized as a role of a correction of the magnetic well effect by the geodesic curvature[14]. The last term of D_G is the geodesic curvature term due to the Pfirsch-Schlüter current. This term always has a destabilizing effect because it is the form of the Schwarz's inequality; $D_G \leq 0$.

We calculate the Mercier criterion for the equilibria in the Large Helical Device (LHD)[10]. The basic machine parameters of the LHD are given in Table 1. Three pairs of axisymmetric poloidal coils are equipped to control the dipole and quadrupole components of the magnetic field and to minimize the leakage flux at the steady state. By controlling of the dipole or vertical component of the axisymmetric poloidal fields we can move the plasma position horizontally changing the magnetic axis in the vacuum field from R_0=3.9m to 3.6m. We define the shift of the position of the vacuum magnetic axis by Δ_v measured from R_0=3.9m. (Changing R_0=3.9m to 3.6m corresponds to Δ_v=0 to −0.3m.) The quadrupole component of the poloidal fields mainly affects the shape of magnetic surfaces. Hereafter

we call the LHD configuration with $\Delta_v = -15$cm and nearly circular toroidally averaged magnetic surfaces 'the standard configuration'. The LHD has been designed to obtain a good single particle confinement, high equilibrium beta, high stability beta, clear magnetic surface, and a possible built-in diverter configuration. The standard configuration satisfies these requirements[10].

We calculate the three dimensional equilibria under the fixed boundary condition. The pressure profile is assumed to be $P = P_0(1-\Phi_{norm})^2$ where Φ_{norm} is the normalized toroidal flux. A fixed profile is given for the net toroidal current density: $J = J_0(1-\Phi_{norm})^2$. We consider the three cases for the total net toroidal current I: a subtractive current of $I = -50$kA (decreasing the rotational transform), $I = 0$kA (currentless equilibrium), and an additive current of $I = +50$kA (increasing the rotational transform).

3 Effect of net toroidal current in the standard configuration

In this section, we study effects of the net toroidal current on the Mercier criterion for the standard configuration of LHD. Figure 1 shows the Mercier unstable regions in the space of ρ and β_0, where $\rho \equiv {\Phi_{norm}}^{1/2} \sim \bar{r}$ ($\bar{r}$ is the normalized average minor radius) and β_0 is the central beta value. Here we assume the existence of the conducting wall at the outermost surface of which the average radius, r_{av}, is 0.575m. Figure 1(a) is the case with a subtractive current of $I = -50$kA (decreasing ι), (b) the case with $I = 0$ (currentless case), and (c) the case with an additive current of $I = +50$kA (increasing ι). In each graph the dot-dashed lines show the boundary between magnetic well and hill regions and dashed lines indicate positions of the rational surfaces. The shaded regions show the Mercier unstable regions in the currentless and the additive current cases. The solid lines in these regions are the contours of the level surface of D_I, which is normalized Mercier criterion defined by

$$D_I \equiv -D_M/\iota^2, \tag{3.1}$$

and the difference of neighboring two level surfaces is $\Delta D_I = 0.1$. The unstable region of the currentless case is very small and the second stability appears in the region above $\beta_0 \sim 8\%$, which corresponds to $\langle\beta\rangle \sim 2.7\%$ for the present pressure profile.

In the case of straight helical configurations the relation between the Suydam criterion and the low-n mode stability limit for the ideal interchange mode was studied by Sugama and Wakatani[16]. They showed that the growth rate of low-n mode can be obtained in the Suydam unstable region. The growth rate of the low-n mode becomes small as the beta value decreases approaching the Suydam limit, and there exists a region near the Suydam limit where the growth rate is too small to be found out numerically. The similar relation between the Mercier criterion and the beta limit by the low-n interchange mode in toroidal geometries for heliotrons and torsatrons was also obtained numerically with the KSTEP code by Nakamura et al.[17], which predicts that the finite growth rates of the low-n modes are found out numerically whenever $D_I \gtrsim 0.2$. Fu et al. also obtained similar relation between the Mercier criterion and the localized low-n modes by using the 3-D

stability code, TERPSICHORE code[18]. The low-n modes may be marginally unstable with very small growth rates in the region with $0 < D_I \lesssim 0.2$. However, such a marginally unstable mode can be easily stabilized by some kinetic effects such as a finite Larmor effect. Therefore, the region with $0 < D_I \lesssim 0.2$ may be thought to be stable for the low-n ideal interchange modes in practice. Based on these considerations, we can say that the currentless standard configuration is actually stable against the low-n modes since only the contour with $D_I = 0.1$ is seen in Fig.1(b).

As is seen in Fig.1(a), if the net toroidal current of 50kA flows in the direction opposite to the helical coil current, which decreases the rotational transform, the standard configuration is completely stabilized against the Mercier modes, hence the low-n ideal interchange modes. On the other hand, the additive net toroidal current flowing in the direction of the helical coil current, which increases the rotational transform, deteriorates the stability. Figure 1(c) of $I = +50$kA (increasing ι) shows wider Mercier unstable region than the currentless case. In this case, some low-n interchange modes may become unstable since there can be seen many Mercier contours with $D_I \geq 0.2$. However, the boundary of the Mercier criterion is closed and the second stability regime persists in the region above $\beta_0 \sim 11\%$ ($\langle\beta\rangle \sim 3.8\%$).

In order to understand the stabilizing mechanism of the subtractive net toroidal current, we examine the equilibrium quantities. Figure 2 shows the profiles of rotational transform for the three cases of $I = -50$kA(decreasing ι), $I = 0$kA(currentless), and $I = +50$kA(increasing ι). In the currentless case, the central rotational transform at very small beta value ($\beta_0 = 0.01\%$) is $\iota_0 = 0.36$ and the edge value is $\iota_a = 1.17$. The additional current of 50kA increases these values to $\iota_0 = 0.47$ and $\iota_a = 1.20$, and the subtractive current of 50kA decreases to $\iota_0 = 0.25$ and $\iota_a = 1.13$. As is known as a general property in the configuration of heliotron/torsatron[19], the central rotational transform ι_0 increases significantly and the edge rotational transform ι_a decreases by a little amount as the beta value increases in the currentless case, and the enhancement of the magnetic shear in the peripheral region is also seen. This tendency is enhanced by the subtractive current decreasing ι and reduced by the additive current increasing ι.

Figure 6(b) shows the Shafranov shift of the equilibria with $I = -50$kA , $I = 0$kA and $I = +50$kA, which is defined by the difference between the major radius of the magnetic axis, R_{ax}, and the major radius of the center of the outermost surface, R_{cnt}, normalized

by the average radius of the outermost surface, r_{av}. It is noted that the reduction in ι_0 by the subtractive current in Fig.2(a) permits a large Shafranov shift during increasing beta value as shown in Fig.6(b), which deepens the magnetic well. Figure 3 shows the magnetic well depth at $\beta_0 = 6\%$, which is defined by

$$(well \quad depth) \equiv \frac{V'(0) - V'(\Phi_{norm})}{V'(0)}. \tag{3.2}$$

The positive gradient of the well depth corresponds to the magnetic well ($V'' < 0$) which is located near the magnetic axis, and the magnetic hill always exists in the peripheral region. The width of the well region is almost independent of the net toroidal current. It should be noted, however, that the absolute value of V'' is enhanced by the subtractive current owing to the large Shafranov shift.

These stabilizing effects due to the magnetic shear and the magnetic well can be understood by estimating the components of the Mercier criterion expressed by Eqs.(2.2) to (2.4). Figure 4 shows the profiles of these components at $\beta_0 = 6\%$ for the currents of $I = -50$kA(decreasing ι), $I = 0$kA(currentless), and $I = +50$kA(increasing ι). In the three cases, the dominant destabilizing effects are due to the D_G term in the central region and the D_{MW} term in the edge region, respectively. The former is stabilized by the magnetic well and the latter is stabilized by the magnetic shear. These stabilizing contributions are enhanced by the subtractive current and reduced by the additive current. There exists a mid region for each equilibrium where D_{MW} and D_G have substantial destabilizing contributions and the magnetic shear stabilization is weak. The Mercier unstable regions are localized in the mid regions, the shaded region in Fig.4(b) and (c), in the currentless and the $I = +50$kA equilibria. In the case of the $I = -50$kA equilibrium, the stabilizing effects of the modified magnetic well and the magnetic shear are strong enough to suppress the destabilizing effects due to D_G even in the mid region.

It is interesting to know whether the net toroidal current I included explicitly in the modified well term stabilizes the mode directly or not. First we divide the D_{MW} into two terms of D_W and $D_{J\cdot B}$ expressed as eqs.(2.12) and (2.13). Figure 5 shows the profiles of these terms for each net toroidal current at $\beta_0 = 6\%$. In the mid region, $D_{J\cdot B}$ term including the net toroidal current effect has a considerable stabilizing contribution in the modified well term for each toroidal current case, while D_W has a destabilizing effect by the magnetic hill. Hence, $D_{J\cdot B}$ term plays a role on extending the region with positive

D_{MW}. This stabilizing effect is also enhanced by the subtractive current. In order to see the role of the net toroidal current, we compare the $D_{J\cdot B}$ term with the D_{NC} term which is the first term of Eq.(2.13) defined by

$$D_{NC} \equiv \iota' I' \left\langle \frac{\mathbf{B}^2}{|\nabla\Phi|^2} \right\rangle. \tag{3.3}$$

The profiles of D_{NC} are also plotted in Fig.5. The $D_{J\cdot B}$ terms have the similar profile for the equilibria with the three kinds of the net toroidal currents. On the other hand, the D_{NC} terms have different profiles according to the direction of the net toroidal current, and the stabilizing contributions of this term in the $D_{J\cdot B}$ term are very small in the mid region. This difference between profiles of the $D_{J\cdot B}$ term and the D_{NC} means that D_{NC} is not a dominant part of the $D_{J\cdot B}$ term at least in the mid region. This result can be understood by the following expression of the current density $\mathbf{J}$:

$$\mathbf{J} = I'\mathbf{B} + \frac{P'}{\mathbf{B}^2}(2\pi B_\theta \mathbf{B} + \mathbf{B} \times \nabla\Phi), \tag{3.4}$$

where B_θ denotes the covariant component in the poloidal direction in the Hamada coordinates [20]. By substituting Eq.(3.4) into Eq.(2.6), it can be easily shown that only the first term includes the net toroidal current explicitly in the expression of Eq.(3.4). The second term of Eq.(3.4) means $\mathbf{J}_\perp$ (the current density perpendicular to $\mathbf{B}$) and the Pfirsch-Schlüter current which are necessary for an MHD equilibrium. The net toroidal current affects this second term only through the change in the equilibrium geometry of the magnetic field. The first term in Eq.(3.4) is canceled out with the D_{NC} term in the $D_{J\cdot B}$ term. Similarly, the terms including the net toroidal current explicitly are canceled in D_G. Hence, no term including I explicitly remains in the Mercier criterion. However, the equilibrium quantities composing the Mercier criterion such as the magnetic shear, the magnetic well, and the Pfirsch-Schlüter current strongly depend on the net toroidal current. As a result, the net toroidal current does not contribute to the Mercier criterion directly although I' appears in Eq.(2.3), but affects the stability only through the change in the geometry of the equilibrium field. This result was obtained for the stellarator expansion method[17]. Here we have confirmed it for three dimensional equilibria.

4 Effect of shifting magnetic axis

The magnetic axis in the LHD configuration can be shifted horizontally keeping the quadrupole component of the magnetic field fixed by controlling the currents in the poloidal field coils. In this case, the relative position of the magnetic axis to the center of the outermost surface is also changed. Figure 6 shows the Shafranov shift in the equilibria with the net toroidal currents of $I = -50$kA, 0kA and +50kA for the case of Δ_v =–5cm, –15cm, and –25cm. First we focus on the currentless cases. Figure 6(b) shows that the major radius of the magnetic axis, R_{ax}, is almost the same as the radius of the center of the outermost surface, R_{cnt}, in the vacuum standard configuration ($\Delta_v = -15$cm). On the other hand, $R_{ax} > R_{cnt}$ in the vacuum configuration of $\Delta_v = -5$cm (outward shift of the magnetic axis), and $R_{ax} < R_{cnt}$ in the vacuum configuration of $\Delta_v = -25$cm (inward shift of the magnetic axis) are seen in Figs.6(a) and 6(c), respectively. It is well-known that the outward shift of the magnetic axis leads to the magnetic well and the inward shift of the axis leads to the magnetic hill. This tendency is seen in Fig. 7 which shows the well depth for the vacuum case of Δ_v =–5cm, –15cm, and –25cm. In the case of $\Delta_v = -5$cm, magnetic well region appears even in the vacuum configuration, while the magnetic hill is enhanced in the case of $\Delta_v = -25$cm. It is also obtained that the magnetic well is more easily formed in the outward shift case, while the magnetic hill region is more extended in the inward shift case at finite beta values than in the standard configuration. These properties strongly affect the Mercier criterion. Figure 8 shows the Mercier unstable regions in the currentless equilibria with Δ_v =–5cm and –25cm. The plasma is stable in the whole region in the $\Delta_v = -5$cm case due to the magnetic well, while there exists lager unstable region in the $\Delta_v = -25$cm case due to the magnetic hill than in the standard configuration.

We have investigated both the effects of the net toroidal currents and shifting magnetic axis on the Mercier criterion. The tendency of the Shafranov shift due to the net toroidal current is qualitatively the same in all the cases of $\Delta_v = -5$cm, -15cm and -25cm. As shown in Fig.6, the Shafranov shifts with the subtractive current of I =–50kA decreasing ϵ are larger than those of the currentless case and those with the additive current is smaller. Therefore, in the cases of Δ_v =–5cm and –25cm, the same effects are seen as those of

the net toroidal currents on the diamagnetic properties such as the magnetic well and the magnetic shear in the standard case are seen.

Figure 9 shows the Mercier unstable regions in the configurations of Δ_v=−5cm and Δ_v=−25cm with the net toroidal currents. In the case of Δ_v=−5cm with the additive current of I =+50kA increasing ι, the unstable region appears in the plasma which is stable in the whole region in the currentless case as shown in Fig.9(a), while the plasma becomes more stable with subtractive current of I = −50kA. In the case of Δ_v=−25cm, the unstable region is reduced by the subtractive current compared with the currentless case as shown in Fig.9(b), while the unstable region is extended by the additive current.

These results are summarized in the diagrams in Fig.10. The Mercier unstable region with the level surfaces of D_I =0.1, 0.2, 0.3, and 0.4 and the equilibrium beta limit are shown in the β_0–Δ_v space. This figure shows that the subtractive current decreasing ι improves the stability against the Mercier mode and the additive current increasing ι deteriorates the stability in the whole range of the position of the magnetic axis. Besides, the tendency that the outward shift of the magnetic axis stabilizes the Mercier mode and the inward shift destabilizes the mode is common for the equilibria with each net toroidal current.

These results mean that the effect of the net toroidal current on the Mercier criterion is almost independently superposed on the effect of the shift of the magnetic axis. This property can be explained by comparing the stabilizing mechanism in the case with the subtractive toroidal current with the one in the case of shifting the magnetic axis outward. The subtractive current changes the poloidal field so that the rotational transform decreases. Hence, it is essential that the Shafranov shift is enhanced by the reduction in ι_0 and the self-stabilizing effect appears at finite beta value. On the other hand, shifting the magnetic axis outward changes the mean toroidal field on each flux surface so that the toroidal field at the axis decreases. Thus the rotational transform at the magnetic axis increases with the outward shift of the axis. This configuration is unfavorable respect to the enhancement of the Shafranov shift. However, the region with the good curvature of field lines is made wider by the outward shift even in the vacuum configuration. It is followed that the magnetic well region easily becomes wide at small beta value, which stabilizes the Mercier mode. After all, the subtractive net current changes the poloidal field and enhances the self-stabilizing effect by the finite beta value, while shifting the magnetic

axis outward changes the mean toroidal field on each flux surface to make the vacuum configuration favorable for the stabilization.

As shown in Fig.10, there exists the second stability regions against the Mercier modes for all of the equilibria with the pressure profile of $P = P_0(1-\Phi_{norm})^2$ and the net toroidal current of $-50\text{kA} \leq I + 50\text{kA}$ in the LHD configuration. In the experiment of ATF device, it was observed that the magnetic fluctuations were reduced in the second stability region for the Mercier criterion in the currentless case[21]. It was shown theoretically that the fluctuations were due to the resistive interchange modes, which were stabilized by the finite beta effects as well as the ideal interchange mode in the second stability region[22]. The ATF result suggests that we may also have a path to the second stability region in LHD if D_I is so small that low-n ideal interchange modes do not appear, because the LHD has a similar magnetic configuration to the ATF. If we can employ the contour of $D_I \simeq 0.2$ as a practical limit for the low-n interchange mode as we have mentioned in Sec.3, the currentless plasma may enter the second stability region through the phase with slight fluctuations in the standard currentless configuration. In order to confirm this expectation for the second stability, it will be desirable to study the nonlinear saturation level of the resistive interchange modes and the stability analysis about the ballooning modes in the Mercier stable region.

Shifting the magnetic axis outward is favorable for the Mercier stability. From a point of view of a single particle orbit loss, however, the more inward shift of the magnetic axis is the more favorable in Fig.10. According to the criterion that $D_I \lesssim 0.2$, we can shift the magnetic axis inward up to $\Delta_v \sim -18\text{cm}$ under the condition that the second stability can be realized. When the subtractive current flows in the plasma column, the second stability can be achieved more easily than in the currentless case. On the other hand, low-n ideal modes prevent the plasma to enter the second stability region in the case of the additive current of 50kA in the range of $-25\text{cm} \leq \Delta_v \leq -5\text{cm}$.

The equilibrium beta limit is also plotted in Fig.10, which is determined by the beta value where the iteration in the VMEC code does not converge. The equilibrium beta limit is reduced by the subtractive current because the Shafranov shift is larger than that in the currentless case, whereas the limit is improved by the additive current.

5 Conclusion

We have investigated the effects of the net toroidal current with a given current density profile on the Mercier criterion for local ideal interchange modes. We have applied the three-dimensional equilibrium code, VMEC code, to the LHD configuration with B_0=3T under the fixed boundary condition and the assumption of the pressure profile $P = P_0(1-\Phi_{norm})^2$. First, in the currentless case, we have obtained the second stability region for the Mercier criterion above $\beta_0 \sim 8\%$ in the standard configuration.

We have found that the effect of the net toroidal current on the Mercier criterion depends on the direction of the current. The stability is improved by the subtractive current which flows in the direction decreasing the rotational transform. The whole plasma region is completely stabilized by the subtractive current of 50kA of which the current density profile is $J = J_0(1 - \Phi_{norm})^2$. In this case, the enhancement of the Shafranov shift due to the decrease in the rotational transform leads to the self-stabilization by the diamagnetic effects. The central and the peripheral regions are more stabilized by the magnetic well and the magnetic shear, respectively, than those in the currentless case. The mid region where the Mercier mode becomes unstable in the currentless case is also stabilized by the combination of the magnetic shear and the modified magnetic well. On the other hand, the additive current increasing the rotational transform deteriorates the stability. It is concluded from these results that the enhancement or reduction of the Shafranov shift due to the change in ι_0 by the net current is essential for altering the stability. These stability properties with the net toroidal current agree with the experimental results by Morimoto et al.[9]. It is noted that although the net toroidal current term is included in the expression of the Mercier criterion explicitly, the term does not affect the stability directly.

It is known that the low-n interchange mode instability appears in the region of $D_I \gtrsim 0.2$. Thus the currentless equilibrium in the standard configuration may be stable against the low-n modes up to the equilibrium limit because we have no region with $D_I > 0.2$. In the LHD standard configuration, the low-n modes may become unstable with $I = +50$kA, while they will be stabilized completely with $I = -50$kA.

We have estimated the Mercier stability of the standard equilibria with the net toroidal

currents of $I = \pm 100$kA. The stabilizing or destabilizing effects are the same as those in the 50kA case qualitatively. We also have studied the stability of the equilibrium with a broad pressure profile of $P = P_0(1 - {\Phi_{norm}}^2)^2$. In the currentless case, the Shafranov shift is smaller, and therefore, the stabilizing effect of the magnetic well is more weak than the equilibrium with the peaked pressure profile used in Secs.3 and 4. Hence the equilibrium is more unstable for the Mercier modes and the region with $D_I > 0.2$ appears. The stabilizing tendency of the net toroidal currents with the same current density profile as in Secs.3 and 4 is similar to that of the peaked pressure equilibria, although the subtractive current of 50kA is not enough to stabilize the modes completely.

The effect of shifting the magnetic axis inward or outward has been investigated. In this case, the effect of the net toroidal current is superposed on the effect of the magnetic axis shift. For instance, in the inward shift case which is unstable against the Mercier criterion in the currentless case, the unstable region can be reduced by the net toroidal current flowing in the direction of decreasing the rotational transform. These results are due to the fact that the net toroidal current and shifting magnetic axis affect different component of the magnetic field on each flux surface, respectively. The subtractive net current changes the poloidal field and enhances the self-stabilizing effect due to the finite beta value, while shifting the magnetic axis outward decreases the mean toroidal field on each flux surface and makes the good curvature region of field lines wide in the vacuum configuration.

We must be careful for the expression of the Mercier criterion in three-dimensional equilibria. Strictly speaking, the Mercier criterion is derived as a stability criterion for each field line on a rational surface[12, 14, 23] and the operator $\langle\ \rangle$ in Eqs.(2.3) and (2.4) should be considered for the average along a field line defined by

$$\langle f \rangle \equiv \oint f \frac{dl}{B}, \tag{5.1}$$

rather than the flux surface defined by (2.7). Based on this estimation, D_M can be different for each field line on the same rational surface, which can also be different from our results estimated by means of the flux-averaged quantities. On the other hand, in the case of $\epsilon/M << 1$ (M is the field period in the toroidal direction.), the same expressions with the flux averages as Eqs.(2.2) to (2.4) can be obtained when we first average the three-dimensional ballooning equation in the toroidal direction by means of the ordering with the parameter $1/M$, and after that, we apply the asymptotic technique to the averaged

equation along a field line[24]. Thus, we can interpret that the expressions of Eqs.(2.2) to (2.4) with the flux averages give the averaged criterion over the label of the field lines on each rational surface. We can see the parameter $\epsilon/M \lesssim 0.1$ in the LHD configuration, which is smaller than unity. Therefore, the differences of D_M between the field lines should be small. Hence, we believe that it is valid to estimate the stability of the LHD equilibria by means of the flux averaged quantities.

In this paper, we are limited to the stability against the ideal interchange modes. However, in order to establish the concept of the second stability against the pressure driven modes completely, stability analyses for the ballooning modes and the effects of the resistivity will be needed. Besides, the current-driven modes may be important even in the heliotron/torsatron configurations if a considerable net toroidal current flows in the plasma column. Effects of the net toroidal current on the ballooning modes and the resistive instabilities are under investigation.

Acknowledgements

We acknowledge for many fruitful discussions with Professor J.Todoroki about the physical mechanism of the magnetic well term in the Mercier criterion and the expression of the Mercier criterion in the three-dimensional case. We thank Dr.J.L.Johnson, Dr.K.Itoh, Dr.V.D.Pustovitov, and Dr.K.Watanabe for some valuable discussions. We also thank Professor A.Iiyoshi for his encouragement.

References

[1] for example, ICHIGUCHI,K., NAKAMURA,Y., WAKATANI,M., YANAGI,N., MORIMOTO,S., Nucl. Fusion **29** (1989) 2093;
NAKAMURA,Y., ICHIGUCHI,K., WAKATANI,M., et al., 'Theory of Fusion Plasmas', Varenna (1990) 6773;
WAKATANI,M., NAKAMURA,Y., ICHIGUCHI,K., Fusion Engi. Design **15** (1992) 395;
GARCIA,L., CARRERAS,B.A., DOMINGUEZ,N., LEBOEUF,J.N., LYNCH,V.E., Phys. Fluids **B2** (1990) 2162.

[2] NAKAJIMA,N., OKAMOTO,M., TODOROKI,J., NAKAMURA,Y., WAKATANI,M., Nucl. Fusion **29** (1989) 605.

[3] SHAING,K.C., CARRERAS,B.A., DOMINGUEZ,N., LYNCH,V.E., TOLLIVER,J.S., Phys. Fluids **B1** (1989) 1663.

[4] WATANABE,K., NAKAJIMA,N., OKAMOTO,M., NAKAMURA,Y., WAKATANI,M., *'Three-Dimensional MHD Equilibrium in the Presence of Bootstrap Current for Large Helical Device (LHD)'* Research Report of National Institute for Fusion Science, NIFS–139, March, 1992 (to be published in Nucl.Fusion).

[5] NAKAJIMA,N., OKAMOTO,M., J. Phys. Soc. Jpn. **61** (1992) 833.

[6] NAKAJIMA,N., OKAMOTO,M., J. Phys. Soc. Jpn. **60** (1991) 4146.

[7] NAKAJIMA,N., OKAMOTO,M., Kakuyugo-Kenkyu **68** (1992) 46.

[8] NAKAJIMA,N., OKAMOTO,M., FUJIWARA,M., *'Physical Mechanism of E_ψ-Driven Current in Asymmetric Toroidal Systems'* submitted to Kakuyugo-Kenkyu.

[9] MORIMOTO,S., YANAGI,N., ICHIGUCHI,K., NAKAMURA,Y., WAKATANI,M., SATO,M., OBIKI,T., IIYOSHI,A., Jpn. J. Appl. Phys. **28** (1989) 1470.

[10] IIYOSHI,A., FUJIWARA,M., MOTOJIMA,O., OYABU,N., YAMAZAKI,K., Fusion Tech. **17** (1990) 148.

[11] HIRSHMAN,S.P., VAN RIJ,W.I., MERKEL,P., Comp. Phys. Comm. **43** (1986) 143.

[12] MERCIER,C., Nucl. Fusion Suppl. Pt.2, (1962) 801.

[13] DOMINGUEZ,N., LEBOEUF,J.N., CARRERAS,B.A., LYNCH,V.E., Nucl. Fusion **29** (1989) 2079.

[14] GLASSER,A.H., GREENE,J.M., JOHNSON,J.L., Phys. Fluids **18** (1975) 875.

[15] JOHNSON,J.L., GREENE,J.M., Plasma Phys. **9** (1967) 611.

[16] SUGAMA,H., WAKATANI,M., J. Phys. Soc. Jpn. **58** (1989) 1128.

[17] NAKAMURA,Y., ICHIGUCHI,K., WAKATANI,M., JOHNSON,J.L., J. Phys. Soc. Jpn. **58** (1989) 3157.

[18] FU,G.Y., COOPER,W.A., GRUBER,R., SCHWENN,U., ANDERSON,D.V., Phys. Fluids **B4** (1992) 1401.

[19] PUSTOVITOV,V.D., SHAFRANOV,V.D., Revs. of Plasma Phys. vol.15, (Consultants Bureau, New York) (1990) 163.

[20] HAMADA,S., Nucl. Fusion **2** (1962) 23.

[21] HARRIS,J.H., MURAKAMI,M., CARRERAS,B.A., et al., Phys. Rev. Lett. **63** (1989) 1249.

[22] CARRERAS,B.A., DOMINGUEZ,N., LEBOEUF,J.N., LYNCH,V.E., CHARLTON,L.A., Oak Ridge National Laboratory Report No.ORNL/TM11102, (1989).

[23] SOLOV'EV,L.S., Sov. Phys. JETP **26** (1968) 1167.

[24] TODOROKI,J., private communication.

Figure Captions

Fig.1 Mercier unstable regions in the LHD standard configuration for (a)$I = -50$kA (decreasing ι), (b)$I = 0$kA(currentless), and (c)$I = +50$kA(increasing ι) cases in (β_0, ρ) plane. Shaded regions show unstable regions. Solid lines in these regions are the contours of the level surface of D_I with the difference of $\Delta D_I = 0.1$. Dot-dashed lines show the boundary between magnetic well and hill regions. Dashed lines indicate the positions of rational surfaces corresponding to ι =1, 4/5, 3/4, 2/3, 3/5, 1/2, 3/7, 2/5, 3/8, 1/3, 3/10 from right to left.

Fig.2 Rotational transform profiles in the standard LHD configuration for (a)$I = -50$kA (decreasing ι), (b)$I = 0$kA(currentless), and (c)$I = +50$kA(increasing ι) cases at $\beta_0 = 0\%$, 2%, 4%, 6% and 8%.

Fig.3 Magnetic well depth in the standard LHD configuration at β_0 =6%. Dashed line shows the case of $I = -50$kA(decreasing ι), solid line shows the case of $I = 0$kA(currentless) and dot-dashed line shows the case of $I = +50$kA(increasing ι).

Fig.4 Profiles of components of Mercier criterion in the standard LHD configuration for (a)$I = -50$kA(decreasing ι), (b)$I = 0$kA(currentless), and (c)$I = +50$kA(increasing ι) cases at $\beta_0 = 6\%$. Solid lines show D_S, dashed lines show D_{MW} and dot-dashed lines show D_G. Shaded regions show unstable regions.

Fig.5 Profiles of D_W, $D_{J\cdot B}$ and D_{NC} in the standard LHD configuration for (a)$I = -50$kA(decreasing ι), (b)$I = 0$kA(currentless), and (c)$I = +50$kA(increasing ι) cases at $\beta_0 = 6\%$. Solid lines show D_W, dashed lines show $D_{J\cdot B}$ and dot-dashed lines show D_{NC}.

Fig.6 Shafranov shifts of the LHD equilibria for (a) $\Delta_v = -5$cm, (b) $\Delta_v = -15$cm, and (c) $\Delta_v = -25$cm. In each graph, dotted line shows the case of $I = -50$kA(decreasing ι), solid line shows the case of $I = 0$kA(currentless), and dot-dashed line shows the case of $I = +50$kA(increasing ι).

Fig.7 Magnetic well depth in the currentless LHD equilibria at β_0 =0.01%. Dashed line shows the case of $\Delta_v = -5$cm, solid line shows the case of $\Delta_v = -15$cm and dot-dashed line shows the case of $\Delta_v = -25$cm.

Fig.8 Mercier unstable regions in the currentless equilibria for (a) $\Delta_v = -5$cm, and (b) $\Delta_v = -25$cm in (β_0, ρ) plane. Shaded regions show unstable regions. Solid lines in these regions are the contours of the level surface of D_I with the difference of $\Delta D_I = 0.1$. Dot-dashed line shows the boundary between magnetic well and hill regions. Dashed lines indicate the positions of rational surfaces corresponding to ι =1, 4/5, 3/4, 2/3, 3/5, 1/2, 3/7, 2/5, 3/8, 1/3, 3/10, 2/7, 1/4, 1/5 from right to left.

Fig.9 Mercier unstable regions in the LHD equilibria for (a) $I = +50$kA(increasing ι) and $\Delta_v = -5$cm, (b) $I = -50$kA(decreasing ι) and $\Delta_v = -25$cm, in (β_0, ρ) plane. Shaded regions show unstable regions. Solid lines in these regions are the contours of the level surface of D_I with the difference of $\Delta D_I = 0.1$. Dot-dashed line shows the boundary between magnetic well and hill regions. Dashed lines indicate the positions of rational surfaces in the same way as in Fig.7.

Fig.10 Mercier stability diagrams in the LHD configuration for (a)$I = -50$kA(decreasing ι), (b)$I = 0$kA(currentless), and (c)$I = +50$kA(increasing ι) cases with the equilibrium limits in (β_0, Δ_v) plane. Dot-shaded regions show unstable regions. Dashed lines in these regions show the contours of the level surface of $D_I = 0.1$, 0.2, 0.3, and 0.4.

Table 1 : Basic machine parameters of the LHD

Pole number of helical coils (ℓ)	2
Number of field period (M)	10
Major radius of herical coils (R_0)	3.9 m
Aspect ratio of helical coils (A_c)	4
Pitch modulation parameter of winding law (α)	0.1
Number of pairs of poloidal field coils	3
Central Magnetic field (B_0)	3 T

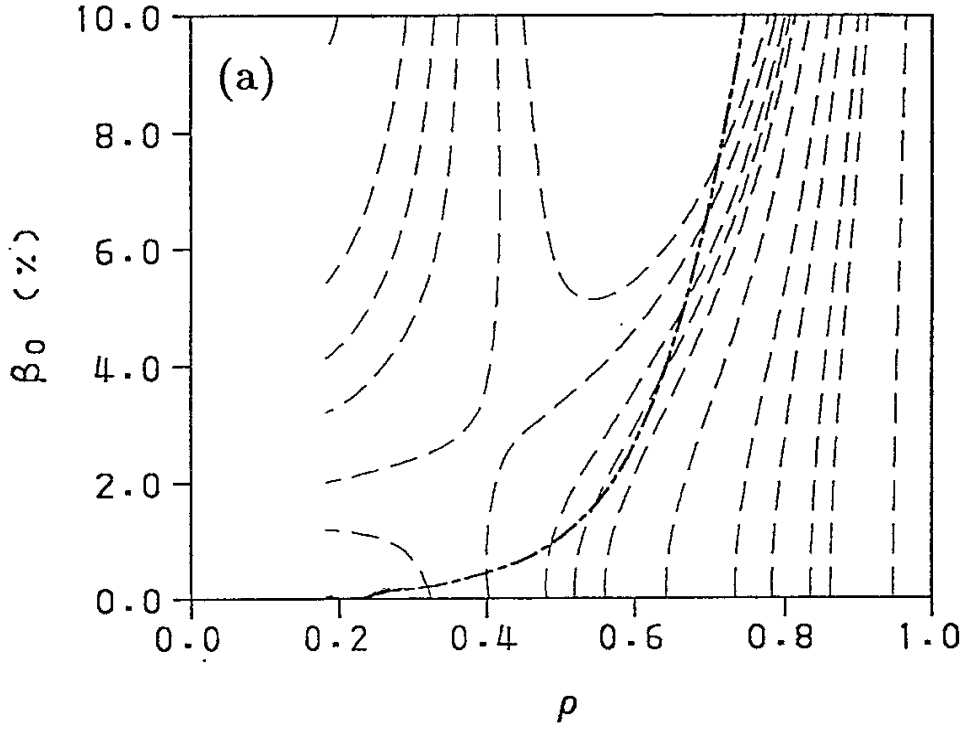

Fig.1 (a)

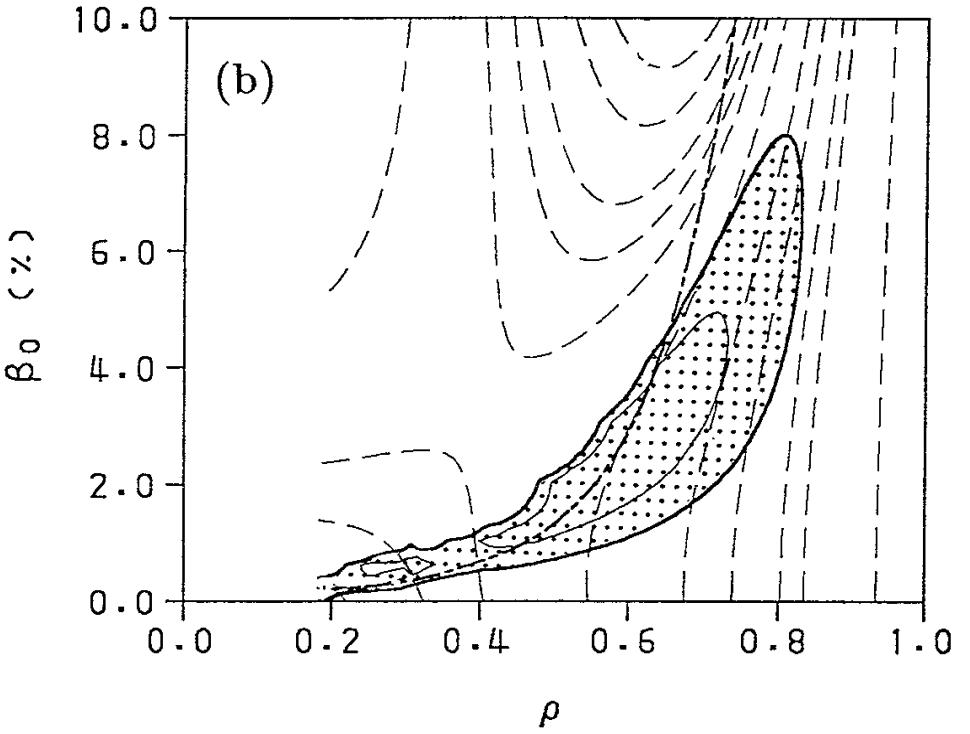

Fig.1 (b)

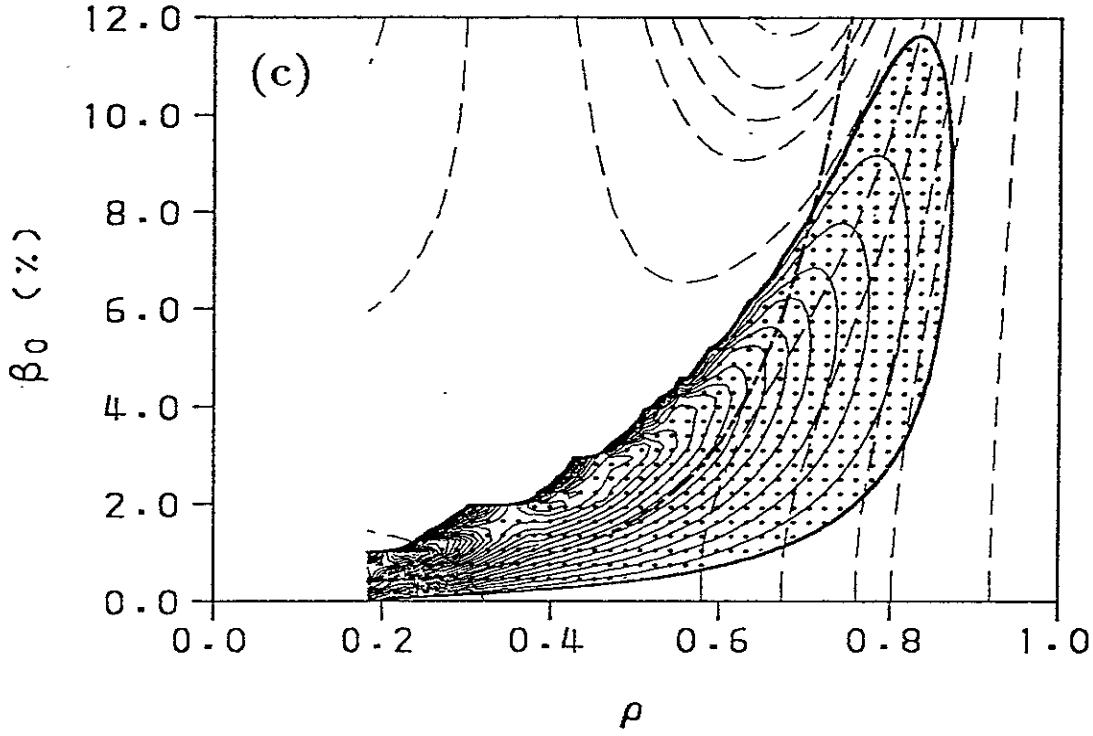

Fig.1 (c)

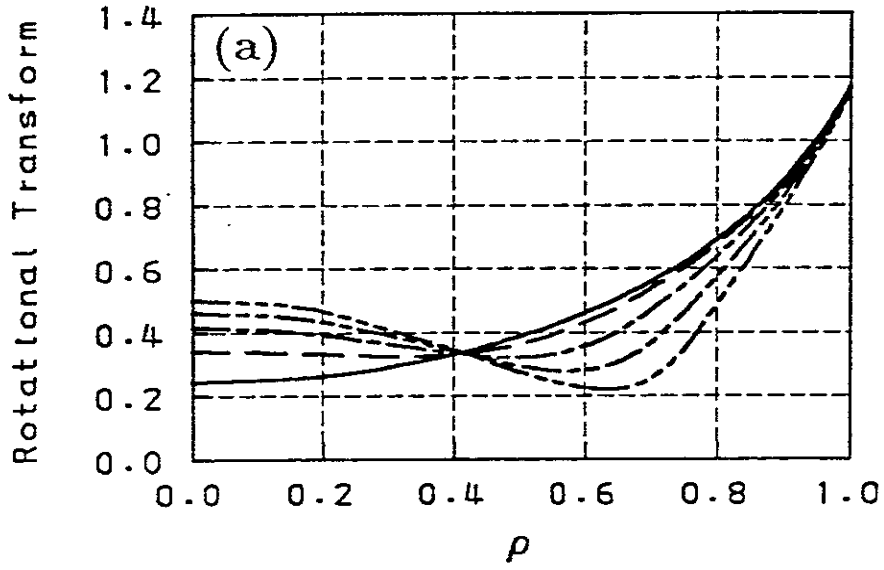
(a)
Rotational Transform
1.4
1.2
1.0
0.8
0.6
0.4
0.2
0.0
0.0
0.2
0.4
0.6
0.8
1.0
ρ

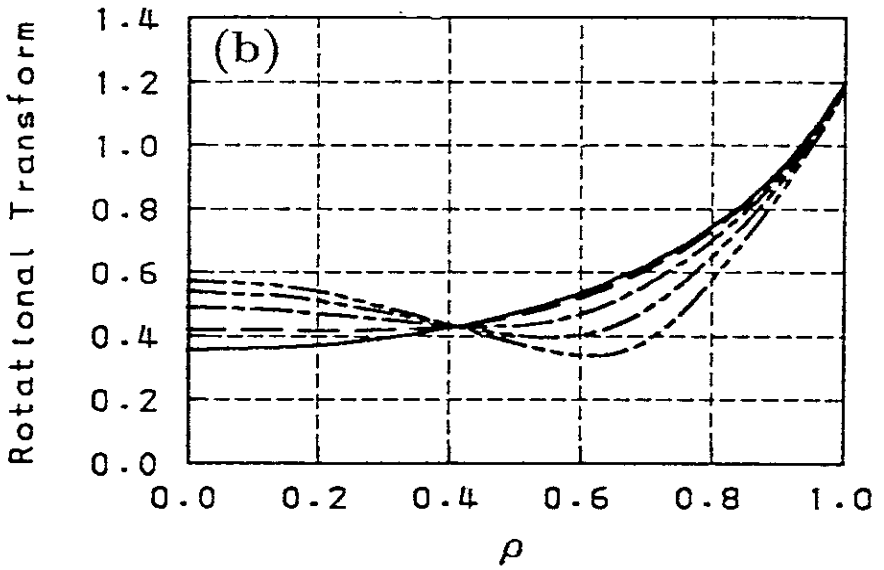
(b)
Rotational Transform
1.4
1.2
1.0
0.8
0.6
0.4
0.2
0.0
0.0
0.2
0.4
0.6
0.8
1.0
ρ

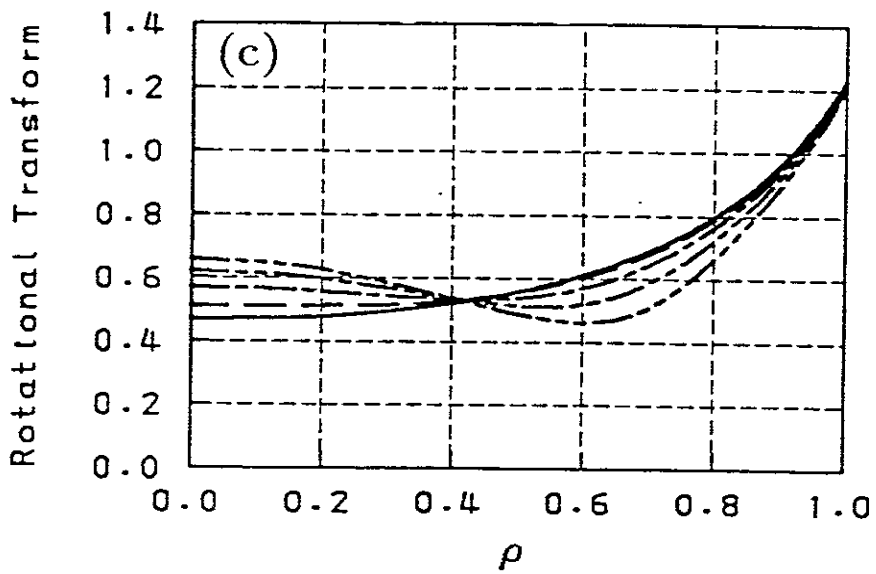
(c)
Rotational Transform
1.4
1.2
1.0
0.8
0.6
0.4
0.2
0.0
0.0
0.2
0.4
0.6
0.8
1.0
ρ

Fig.2

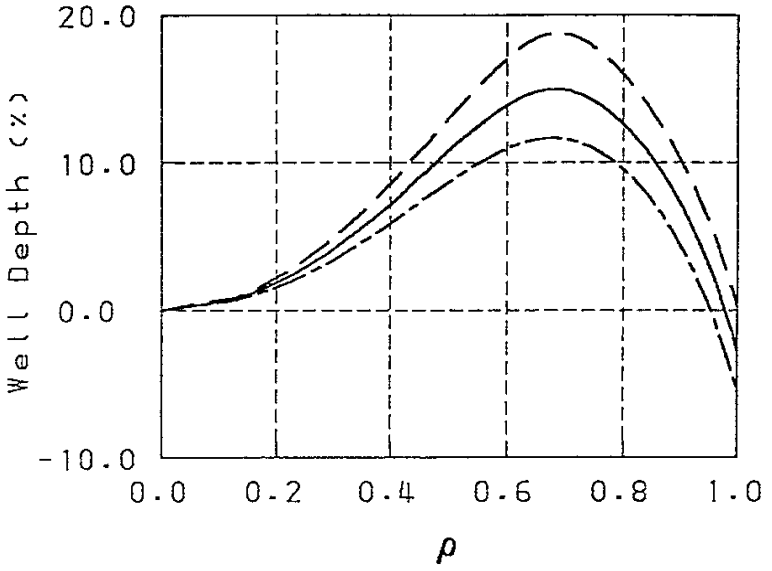

Fig.3

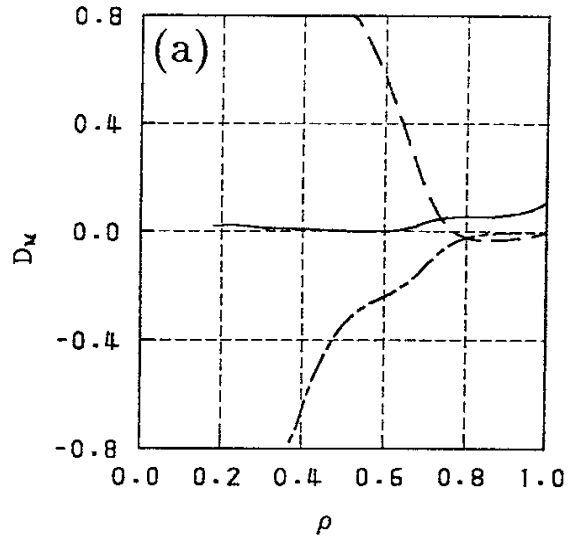
(a)
0.8
0.4
0.0
-0.4
-0.8
D_M
0.0 0.2 0.4 0.6 0.8 1.0
ρ

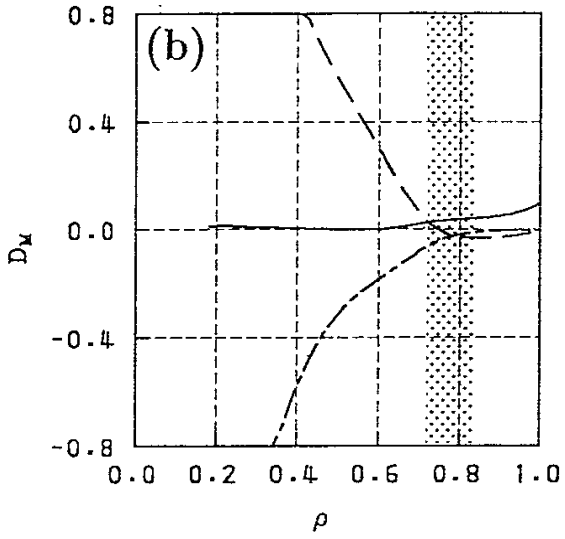
(b)
0.8
0.4
0.0
-0.4
-0.8
D_M
0.0 0.2 0.4 0.6 0.8 1.0
ρ

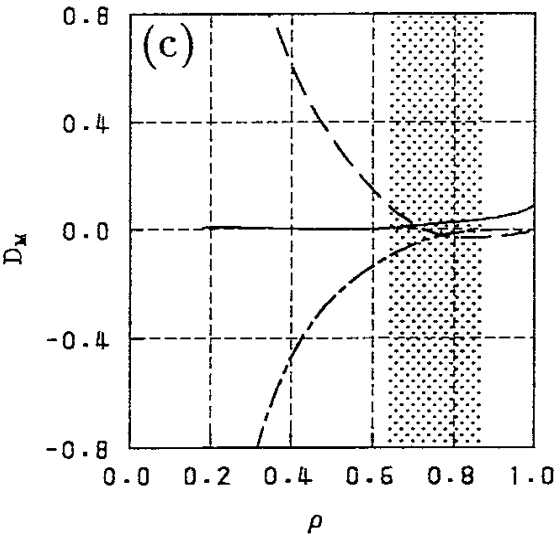
(c)
0.8
0.4
0.0
-0.4
-0.8
D_M
0.0 0.2 0.4 0.6 0.8 1.0
ρ

Fig.4

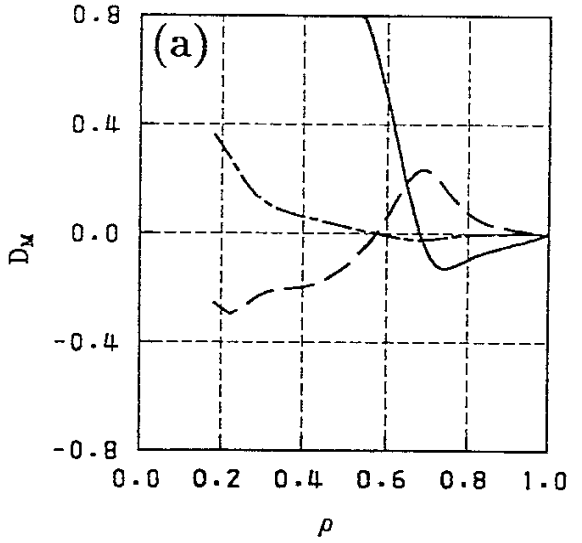
(a)
0.8
0.4
0.0
-0.4
-0.8
D_M
0.0 0.2 0.4 0.6 0.8 1.0
ρ

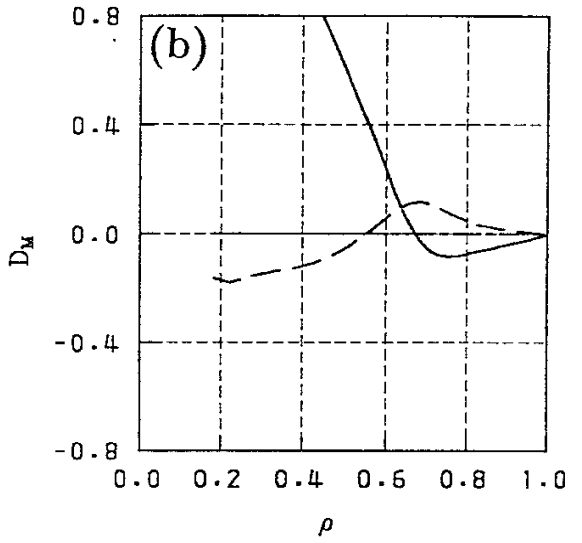
(b)
0.8
0.4
0.0
-0.4
-0.8
D_M
0.0 0.2 0.4 0.6 0.8 1.0
ρ

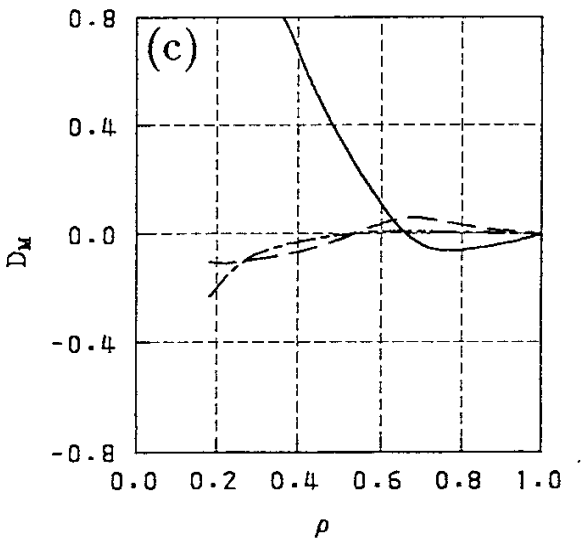
(c)
0.8
0.4
0.0
-0.4
-0.8
D_M
0.0 0.2 0.4 0.6 0.8 1.0
ρ

Fig.5

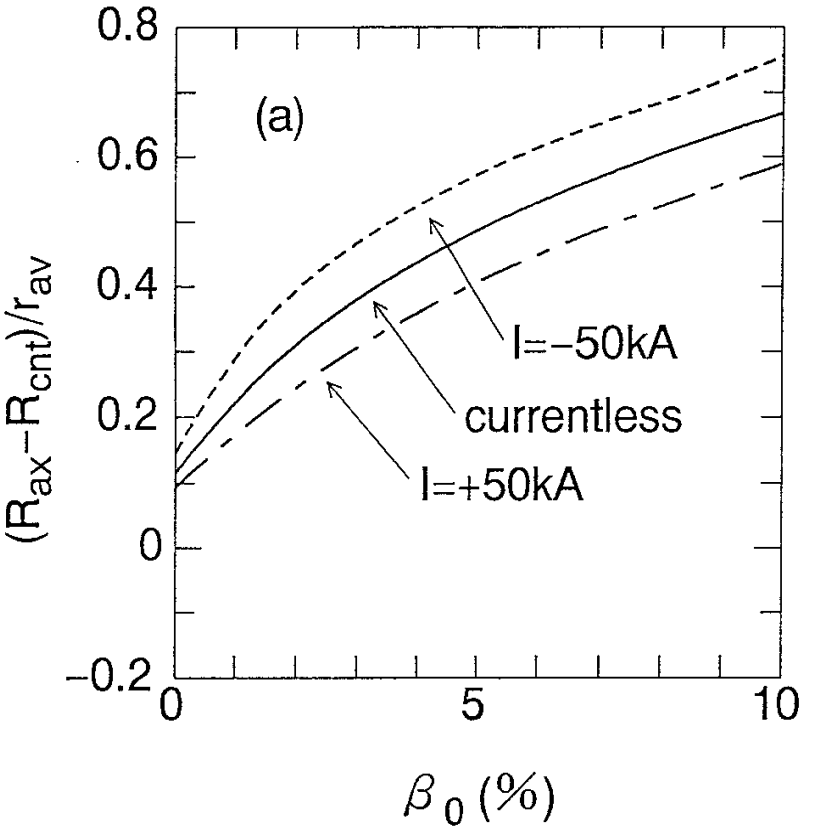
0.8
0.6
0.4
0.2
0
−0.2
0
5
10
(a)
I=−50kA
currentless
I=+50kA
$(R_{ax}-R_{cnt})/r_{av}$
β_0 (%)

Fig.6 (a)

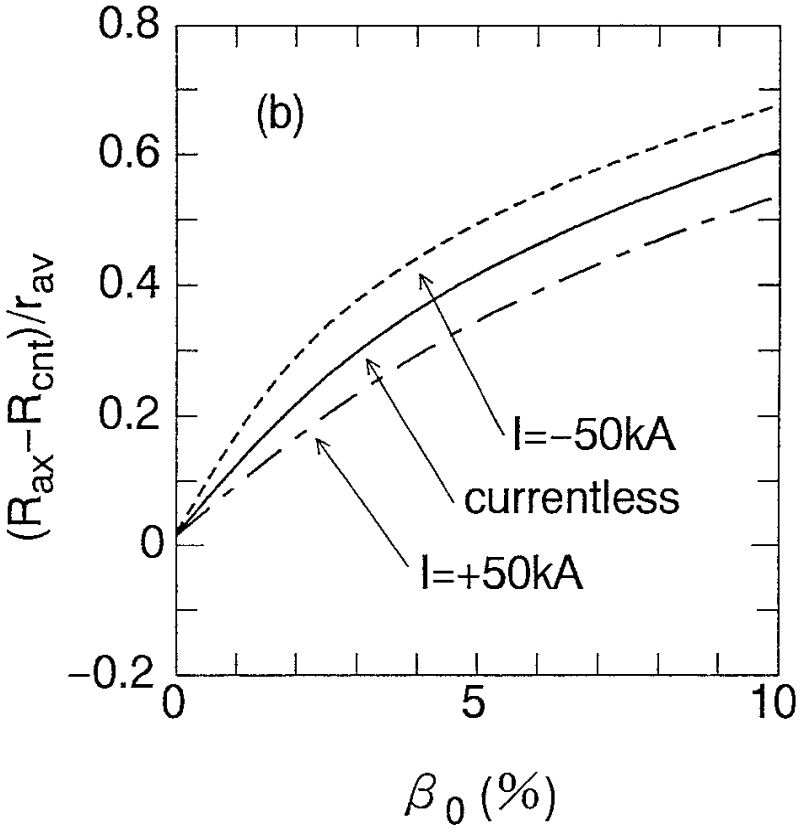
0.8
0.6
0.4
0.2
0
−0.2
0
5
10
(b)
I=−50kA
currentless
I=+50kA
$(R_{ax}-R_{cnt})/r_{av}$
β_0 (%)

Fig.6 (b)

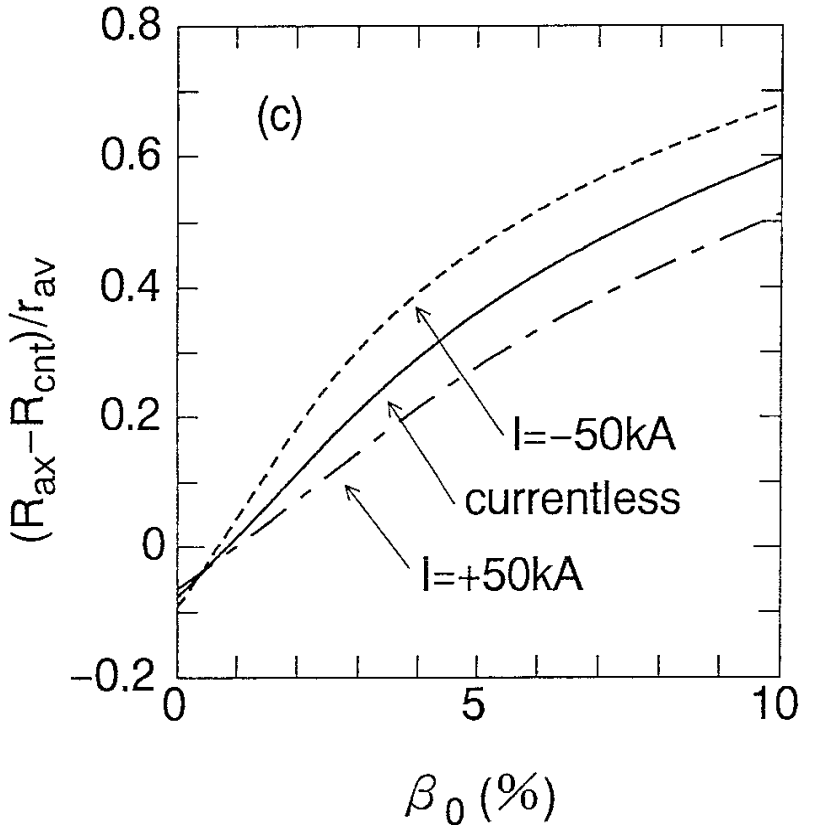
0.8
0.6
0.4
0.2
0
−0.2
0
5
10
(c)
I=−50kA
currentless
I=+50kA
$(R_{ax}-R_{cnt})/r_{av}$
β_0 (%)

Fig.6 (c)

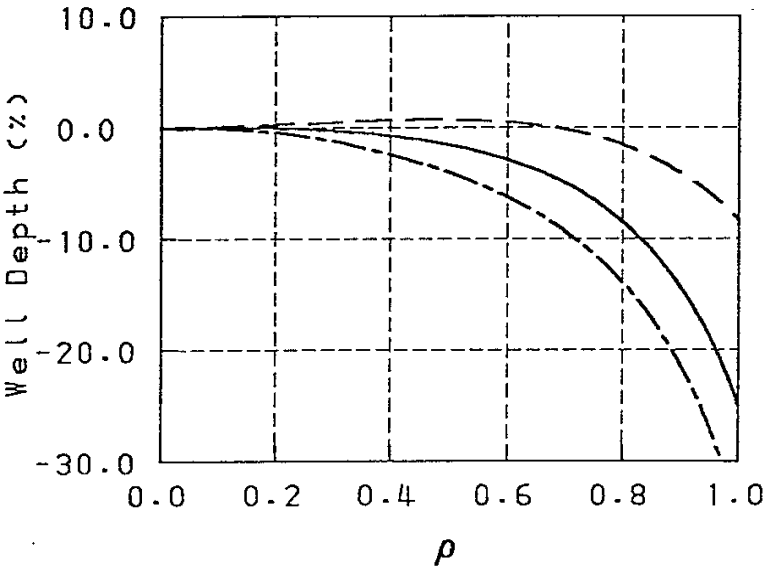

Fig.7

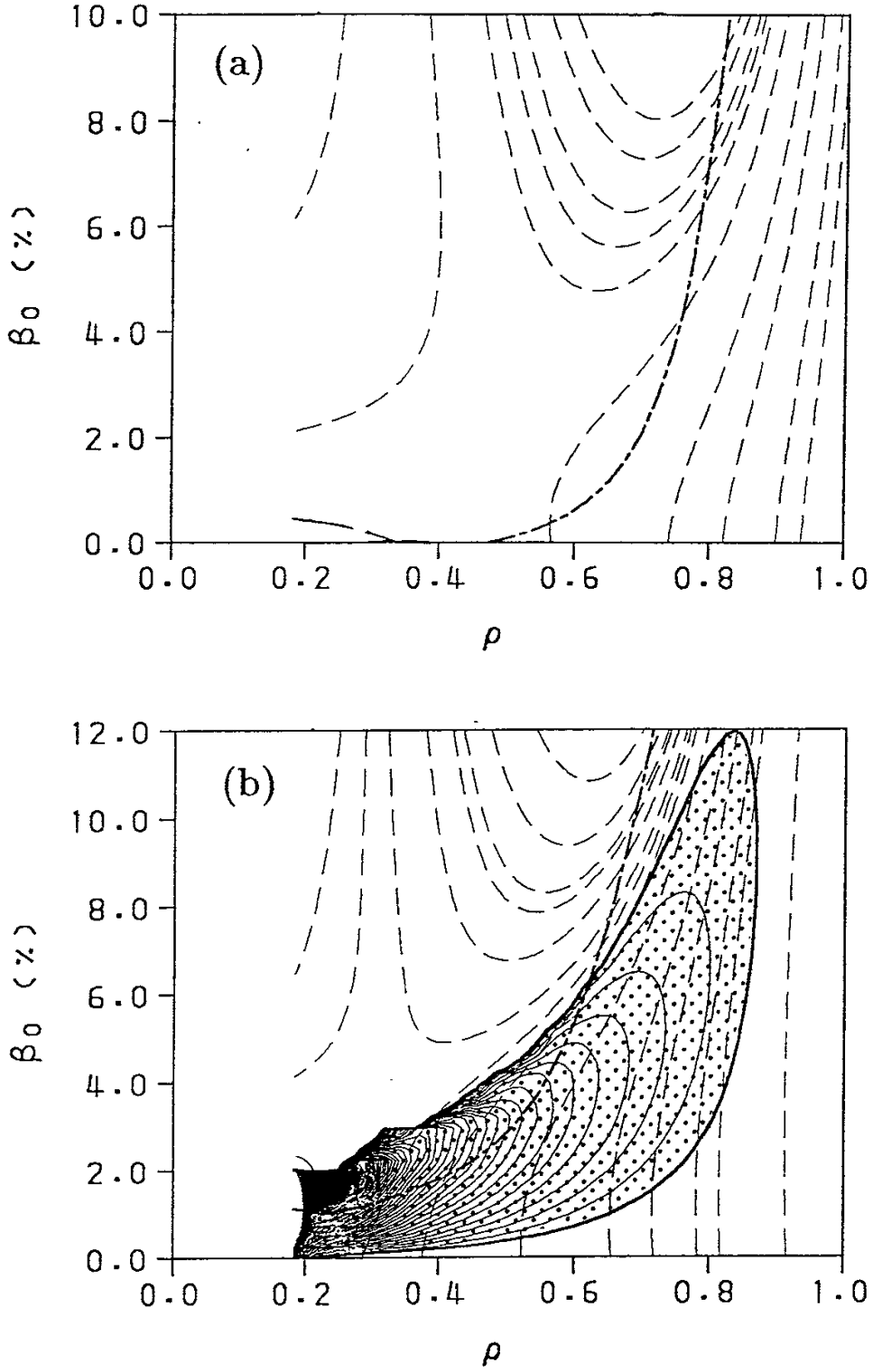
(a)
10.0
8.0
6.0
4.0
2.0
0.0
β_0 (%)
0.0
0.2
0.4
0.6
0.8
1.0
ρ
(b)
12.0
10.0
8.0
6.0
4.0
2.0
0.0
β_0 (%)
0.0
0.2
0.4
0.6
0.8
1.0
ρ

Fig.8

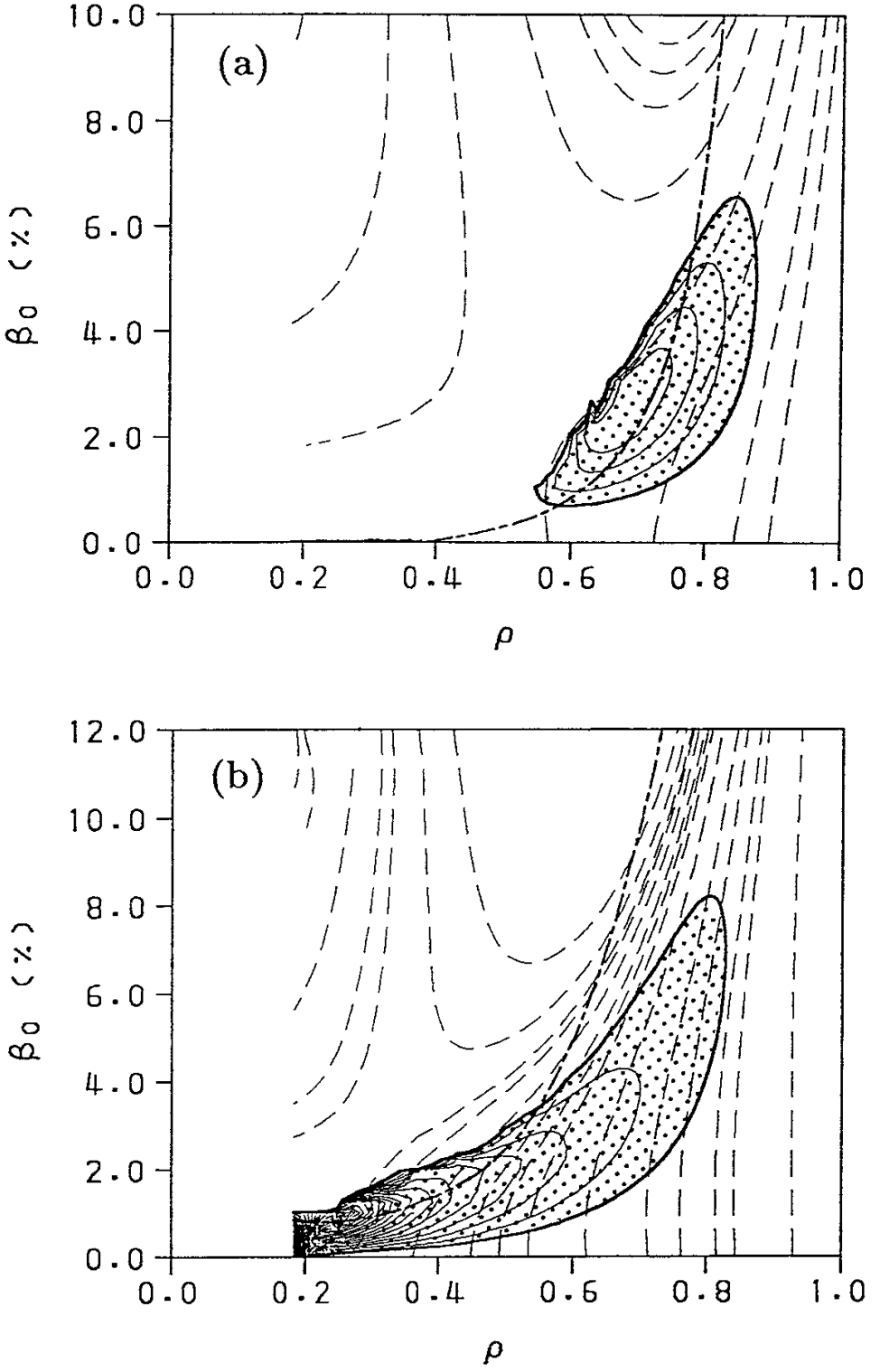
(a)
10.0
8.0
6.0
4.0
2.0
0.0
β_0 (%)
0.0
0.2
0.4
0.6
0.8
1.0
ρ
(b)
12.0
10.0
8.0
6.0
4.0
2.0
0.0
β_0 (%)
0.0
0.2
0.4
0.6
0.8
1.0
ρ

Fig.9

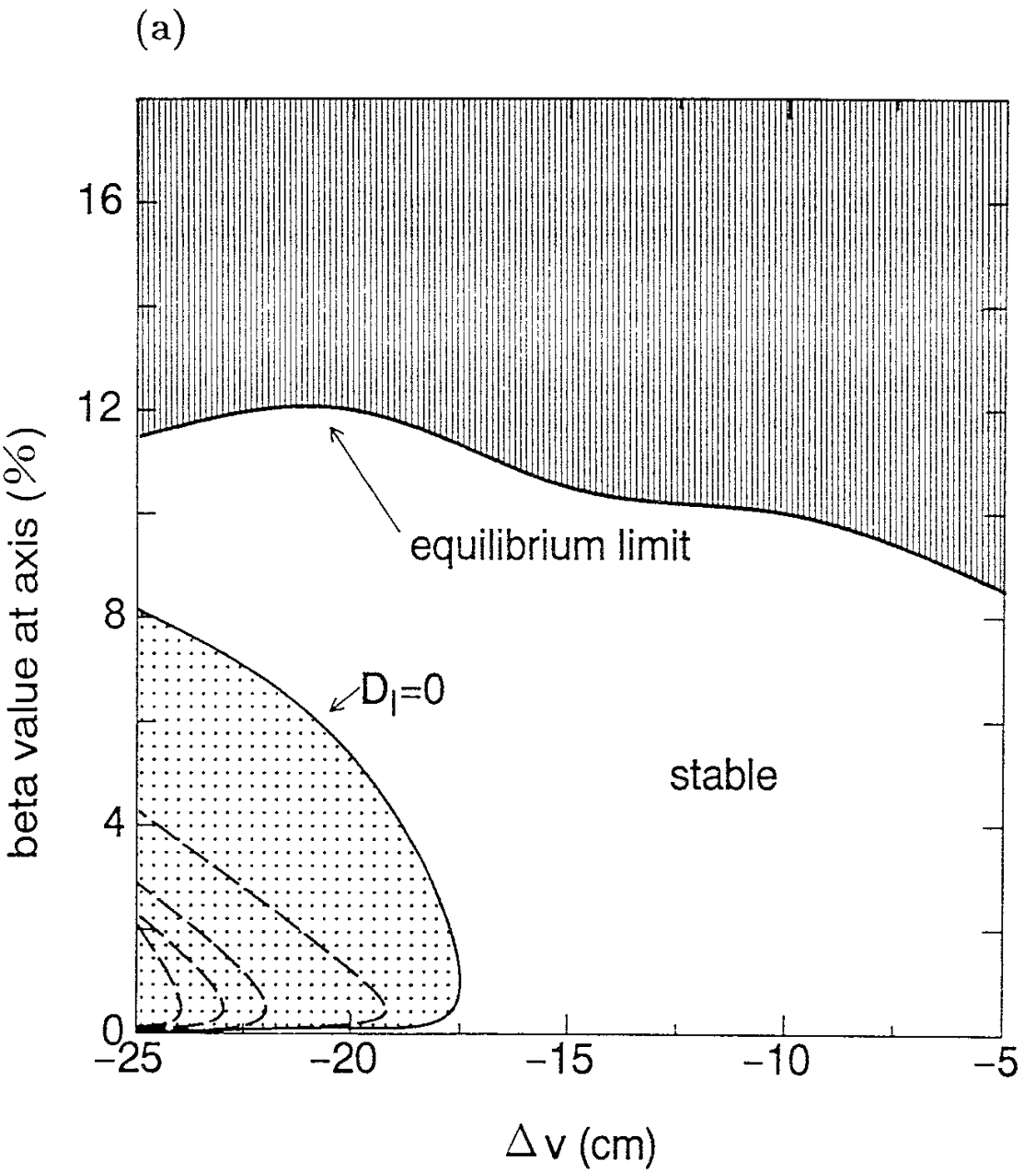
(a)
16
12
8
4
0
beta value at axis (%)
equilibrium limit
D_I=0
stable
−25
−20
−15
−10
−5
Δv (cm)

Fig.10 (a)

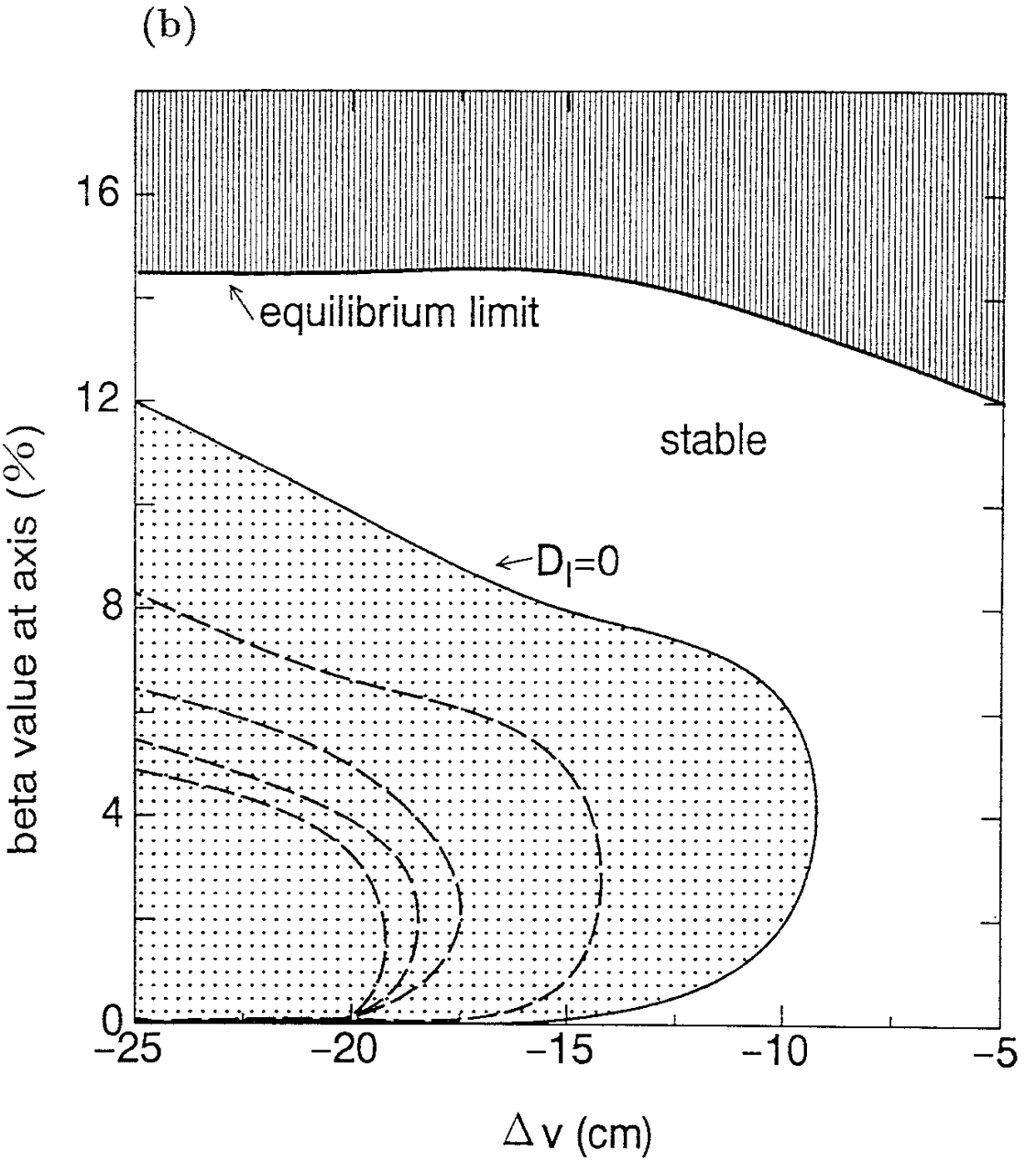
(b)
16
12
8
4
0
beta value at axis (%)
equilibrium limit
stable
D_I=0
−25
−20
−15
−10
−5
Δv (cm)

Fig.10 (b)

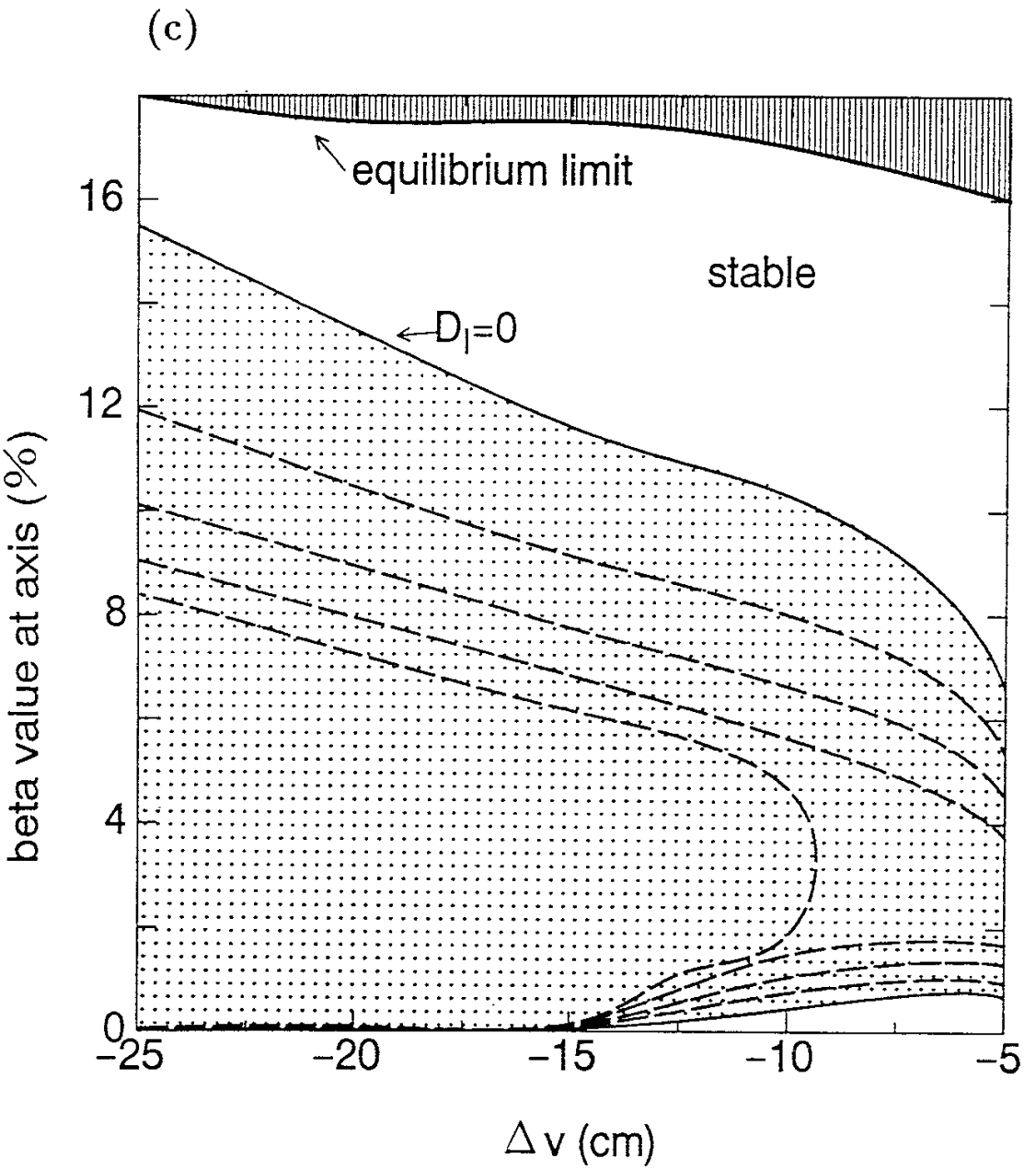
(c)
equilibrium limit
stable
D_I=0
16
12
8
4
0
−25
−20
−15
−10
−5
beta value at axis (%)
Δ v (cm)

Fig.10 (c)

Recent Issues of NIFS Series

NIFS-123 Y. Kondoh, *Relaxed State of Energy in Incompressible Fluid and Incompressible MHD Fluid* ; Dec. 1991

NIFS-124 K. Ida, S. Hidekuma, M. Kojima, Y. Miura, S. Tsuji, K. Hoshino, M. Mori, N. Suzuki, T. Yamauchi and JFT-2M Group, *Edge Poloidal Rotation Profiles of H-Mode Plasmas in the JFT-2M Tokamak ;* Dec. 1991

NIFS-125 H. Sugama and M. Wakatani, *Statistical Analysis of Anomalous Transport in Resistive Interchange Turbulence* ;Dec. 1991

NIFS-126 K. Narihara, *A Steady State Tokamak Operation by Use of Magnetic Monopoles* ; Dec. 1991

NIFS-127 K. Itoh, S. -I. Itoh and A. Fukuyama, *Energy Transport in the Steady State Plasma Sustained by DC Helicity Current Drive* ;Jan. 1992

NIFS-128 Y. Hamada, Y. Kawasumi, K. Masai, H. Iguchi, A. Fujisawa, JIPP T-IIU Group and Y. Abe, *New Hight Voltage Parallel Plate Analyzer* ; Jan. 1992

NIFS-129 K. Ida and T. Kato, *Line-Emission Cross Sections for the Charge-exchange Reaction between Fully Stripped Carbon and Atomic Hydrogen in Tokamak Plasma*; Jan. 1992

NIFS-130 T. Hayashi, A. Takei and T. Sato, *Magnetic Surface Breaking in 3D MHD Equilibria of l=2 Heliotron* ; Jan. 1992

NIFS-131 K. Itoh, K. Ichiguchi and S. -I. Itoh, *Beta Limit of Resistive Plasma in Torsatron/Heliotron* ; Feb. 1992

NIFS-132 K. Sato and F. Miyawaki, *Formation of Presheath and Current-Free Double Layer in a Two-Electron-Temperature Plasma* ; Feb. 1992

NIFS-133 T. Maruyama and S. Kawata, *Superposed-Laser Electron Acceleration* Feb. 1992

NIFS-134 Y. Miura, F. Okano, N. Suzuki, M. Mori, K. Hoshino, H. Maeda, T. Takizuka, JFT-2M Group, S.-I. Itoh and K. Itoh, *Rapid Change of Hydrogen Neutral Energy Distribution at L/H-Transition in JFT-2M H-mode ;* Feb. 1992

NIFS-135 H. Ji, H. Toyama, A. Fujisawa, S. Shinohara and K. Miyamoto *Fluctuation and Edge Current Sustainment in a Reversed-Field-*

Pinch; Feb. 1992

NIFS-136 K. Sato and F. Miyawaki, *Heat Flow of a Two-Electron-Temperature Plasma through the Sheath in the Presence of Electron Emission;* Mar. 1992

NIFS-137 T. Hayashi, U. Schwenn and E. Strumberger, *Field Line Diversion Properties of Finite ß Helias Equilibria;* Mar. 1992

NIFS-138 T. Yamagishi, *Kinetic Approach to Long Wave Length Modes in Rotating Plasmas*; Mar. 1992

NIFS-139 K. Watanabe, N. Nakajima, M. Okamoto, Y. Nakamura and M. Wakatani, *Three-dimensional MHD Equilibrium in the Presence of Bootstrap Current for Large Helical Device (LHD)*; Mar. 1992

NIFS-140 K. Itoh, S. -I. Itoh and A. Fukuyama, *Theory of Anomalous Transport in Toroidal Helical Plasmas;* Mar. 1992

NIFS-141 Y. Kondoh, *Internal Structures of Self-Organized Relaxed States and Self-Similar Decay Phase;* Mar. 1992

NIFS-142 U. Furukane, K. Sato, K. Takiyama and T. Oda, *Recombining Processes in a Cooling Plasma by Mixing of Initially Heated Gas*; Mar. 1992

NIFS-143 Y. Hamada, K. Masai, Y. Kawasumi, H. Iguchi, A. Fijisawa and JIPP T-IIU Group, *New Method of Error Elimination in Potential Profile Measurement of Tokamak Plasmas by High Voltage Heavy Ion Beam Probes;* Apr. 1992

NIFS-144 N. Ohyabu, N. Noda, Hantao Ji, H. Akao, K. Akaishi, T. Ono, H. Kaneko, T. Kawamura, Y. Kubota, S. Morimoto. A. Sagara, T. Watanabe, K. Yamazaki and O. Motojima, *Helical Divertor in the Large Helical Device;* May 1992

NIFS-145 K. Ohkubo and K. Matsumoto, *Coupling to the Lower Hybrid Waves with the Multijunction Grill*; May 1992

NIFS-146 K. Itoh, S. -I.Itoh, A. Fukuyama, S. Tsuji and Allan J. Lichtenberg, *A Model of Major Disruption in Tokamaks*; May 1992

NIFS-147 S. Sasaki, S. Takamura, M. Ueda, H. Iguchi, J. Fujita and K. Kadota, *Edge Plasma Density Reconstruction for Fast Monoenergetic Lithium Beam Probing*; May 1992

NIFS-148 N. Nakajima, C. Z. Cheng and M. Okamoto, *High-n Helicity-induced*

Shear Alfvén Eigenmodes; May 1992

NIFS-149 A. Ando, Y. Takeiri, O. Kaneko, Y. Oka, M. Wada, and T. Kuroda, *Production of Negative Hydrogen Ions in a Large Multicusp Ion Source with Double-Magnetic Filter Configuration*; May 1992

NIFS-150 N. Nakajima and M. Okamoto, *Effects of Fast Ions and an External Inductive Electric Field on the Neoclassical Parallel Flow, Current, and Rotation in General Toroidal Systems*; May 1992

NIFS-151 Y. Takeiri, A. Ando, O. Kaneko, Y. Oka and T. Kuroda, *Negative Ion Extraction Characteristics of a Large Negative Ion Source with Double-Magnetic Filter Configuration*; May 1992

NIFS-152 T. Tanabe, N. Noda and H. Nakamura, *Review of High Z Materials for PSI Applications* ; Jun. 1992

NIFS-153 Sergey V. Bazdenkov and T. Sato, *On a Ballistic Method for Double Layer Regeneration in a Vlasov-Poisson Plasma*; Jun. 1992

NIFS-154 J. Todoroki, *On the Lagrangian of the Linearized MHD Equations*; Jun. 1992

NIFS-155 K. Sato, H. Katayama and F. Miyawaki, *Electrostatic Potential in a Collisionless Plasma Flow Along Open Magnetic Field Lines;* Jun. 1992

NIFS-156 O.J.W.F.Kardaun, J.W.P.F.Kardaun, S.-I. Itoh and K. Itoh, *Discriminant Analysis of Plasma Fusion Data*; Jun. 1992

NIFS-157 K. Itoh, S.-I. Itoh, A. Fukuyama and S. Tsuji, *Critical Issues and Experimental Examination on Sawtooth and Disruption Physics*; Jun. 1992

NIFS-158 K. Itoh and S.-I. Itoh, *Transition to H-Mode by Energetic Electrons*; July 1992

NIFS-159 K. Itoh, S.-I. Itoh and A. Fukuyama, *Steady State Tokamak Sustained by Bootstrap Current Without Seed Current*; July 1992

NIFS-160 H. Sanuki, K. Itoh and S.-I. Itoh, *Effects of Nonclassical Ion Losses on Radial Electric Field in CHS Torsatron/Heliotron*; July 1992

NIFS-161 O. Motojima, K. Akaishi, K. Fujii, S. Fujiwaka, S. Imagawa, H. Ji, H. Kaneko, S. Kitagawa, Y. Kubota, K. Matsuoka, T. Mito, S. Morimoto, A. Nishimura, K. Nishimura, N. Noda, I. Ohtake, N. Ohyabu, S. Okamura, A. Sagara, M. Sakamoto, S. Satoh, T. Satow, K. Takahata, H. Tamura, S. Tanahashi, T. Tsuzuki, S. Yamada, H. Yamada, K. Yamazaki, N. Yanagi, H. Yonezu, J. Yamamoto, M. Fujiwara and

A. Iiyoshi, *Physics and Engineering Design Studies on Large Helical Device*; Aug. 1992

NIFS-162 V. D. Pustovitov, *Refined Theory of Diamagnetic Effect in Stellarators;* Aug. 1992

NIFS-163 K. Itoh, *A Review on Application of MHD Theory to Plasma Boundary Problems in Tokamaks*; Aug. 1992

NIFS-164 Y.Kondoh and T.Sato, *Thought Analysis on Self-Organization Theories of MHD Plasma*; Aug. 1992

NIFS-165 T. Seki, R. Kumazawa, T. Watari, M. Ono, Y. Yasaka, F. Shimpo, A. Ando, O. Kaneko, Y. Oka, K. Adati, R. Akiyama, Y. Hamada, S. Hidekuma, S. Hirokura, K. Ida, A. Karita, K. Kawahata, Y. Kawasumi, Y. Kitoh, T. Kohmoto, M. Kojima, K. Masai, S. Morita, K. Narihara, Y. Ogawa, K. Ohkubo, S. Okajima, T. Ozaki, M. Sakamoto, M. Sasao, K. Sato, K. N. Sato, H. Takahashi, Y. Taniguchi, K. Toi and T. Tsuzuki, *High Frequency Ion Bernstein Wave Heating Experiment on JIPP T-IIU Tokamak*; Aug. 1992

NIFS-166 Vo Hong Anh and Nguyen Tien Dung, *A Synergetic Treatment of the Vortices Behaviour of a Plasma with Viscosity*; Sep. 1992

NIFS-167 K. Watanabe and T. Sato, *A Triggering Mechanism of Fast Crash in Sawtooth Oscillation*; Sep. 1992

NIFS-168 T. Hayashi, T. Sato, W. Lotz, P. Merkel, J. Nührenberg, U. Schwenn and E. Strumberger, *3D MHD Study of Helias and Heliotron;* Sep. 1992

NIFS-169 N. Nakajima, K. Ichiguchi, K. Watanabe, H. Sugama, M. Okamoto, M. Wakatani, Y. Nakamura and C. Z. Cheng, *Neoclassical Current and Related MHD Stability, Gap Modes, and Radial Electric Field Effects in Heliotron and Torsatron Plasmas;* Sep. 1992

NIFS-170 H. Sugama, M. Okamoto and M. Wakatani, *K- ε Model of Anomalous Transport in Resistive Interchange Turbulence* ; Sep, 1992

NIFS-171 H. Sugama, M. Okamoto and M. Wakatani, *Vlasov Equation in the Stochastic Magnetic Field* ; Sep. 1992

NIFS-172 N. Nakajima, M. Okamoto and M. Fujiwara, *Physical Mechanism of E_{ψ}-Driven Current in Asymmetric Toroidal Systems* ; Sep.1992

NIFS-173 N. Nakajima, J. Todoroki and M. Okamoto, *On Relation between Hamada and Boozer Magnetic Coordinate System* ; Sep. 1992